ALGORITHM DEVELOPMENT AND *IN SITU* DATA COLLECTION FOR SGLI OCEAN COLOR REMOTE SENSING (JX-PSPC-515384) – R. Frouin (PI) and Jing Tan, SIO/UCSD, C. Dupouy, IRD (Co-I)

Abstract. During JFY 2021, i.e., Year 3 of JX-PSPC-515384 investigation, we have 1) continued our work on estimating the fraction of PAR absorbed by live phytoplankton from linear combination of water reflectance and 2) investigated the relationship between degree of polarization of water reflectance at 673 nm and particle assemblages. Specifically, we have used simulated data to test parametric and non-parametric APAR models of various complexity, we have examined the seasonal and interannual variability of APAR in the Northeast Asia Seas during the first 47-year of the mission, and we have related degree of polarization to chlorophyll concentration and total suspended matter in selected SGLI imagery. The results showed that other absorbers than chlorophyll and their temporal distribution may significantly influence the characteristics of APAR seasonal variability. They provided evidence that the relation between degree of polarization and particle concentrations is not unique but modulated by the nature of the assemblages (organic/inorganic). We have also prepared for the upcoming (March-April 2022) SOKOWASA bio-optical cruise in the South Pacific.

1. Estimating APAR from water reflectance

Parametric and non-parametric APAR models

-A variety of APAR methods were tested on simulated data: (Parametric) Chla-based and multilinear combinations of R_w/Rw_0; (Non-Parametric) Neural network, gradient boosting, Nearest-Neighbor, Kernel, Random Forest, Generalized Additive Models.

-Simulated Data: IOCCG and PACE IOPs, vertically homogeneous and heterogeneous situations, i.e., 2912 cases. Typical atmospheric correction noise added to data.

-Data set separated into training and validation parts (2/3 and 1/3). Average models obtained from N random realizations of the training data sets.

-Evaluation against in situ data acquired during various campaigns worldwide (393 pairs of APAR and R_w).

Performance statistics of various APAR models

Without AC Noise

Algorithm	Bias	RMS	R^2	N
R_w/R_{w0}	-0.000 (-0.0%)	0.083 (42.8%)	0.566	2912
Class-based R_w/R_{w0}	-0.000 (-0.0%)	0.055 (28.5%)	0.808	2912
Neural network	-0.000 (-0.2%)	0.031 (15.7%)	0.942	2912
KNN regression	0.000 (0.0%)	0.010 (4.9%)	0.994	2912
Kernel regression	0.000 (0.0%)	0.019 (9.8%)	0.978	2912
Gradient boost regression	-0.000 (-0.3%)	0.036 (18.6%)	0.920	2912
Random forest regression	-0.000 (-0.1%)	0.051 (26.3%)	0.848	2912
GAM/PC, 2 PCs	-0.000 (-0.0%)	0.032 (16.7%)	0.934	2912
GAM/PC, 3 PCs	0.000 (0.1 %)	0.019 (9.8%)	0.977	2912
GAM/log(Chla), log(f_b)	-0.000 (-0.0%)	0.037 (18.9%)	0.915	2912

With AC Noise

Algorithm	Bias	RMS	R^2	N
R_w/R_{w0}	0.000 (0.0%)	0.084 (43.0%)	0.564	2912
Class-based R_w/R_{w0}	-0.000 (-0.0%)	0.060 (30.6%)	0.779	2912
Neural network	-0.000 (-0.1%)	0.037 (19.0%)	0.915	2912
KNN regression	-0.002 (-0.8%)	0.072 (37.1%)	0.676	2912
Kernel regression	-0.001 (-0.5%)	0.059 (30.3%)	0.791	2912
Gradient boost regression	-0.000 (-0.3%)	0.045 (23.1%)	0.877	2912
Random forest regression	0.000 (0.1%)	0.069 (35.3%)	0.716	2912
GAM/PC, 2 PCs	0.000 (0.0%)	0.042 (21.6%)	0.890	2912
GAM/PC, 3 PCs	0.000 (0.1 %)	0.031 (16.1%)	0.939	2912
GAM/log(Chla), log(f_b)	0.000 (0.1%)	0.044 (22.5%)	0.881	2912

-Some models, i.e., NN and Kernel, perform very well without noise, but they are highly sensitive to atmospheric correction noise.

-Robustness of class-based parametric and non-parametric models is not sufficient for operational application to SGLI data. Simulated dataset does not fully capture expected situations.

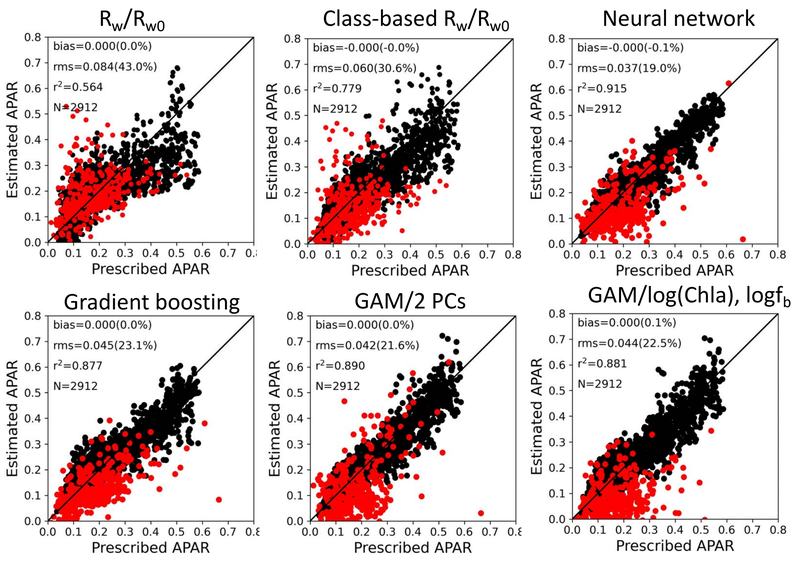

-Non-parametric models provided better results on simulated data with AC noise than parametric models.

-Application of theoretical models with AC noise to in situ data reveals relatively large biases for GAMs.

-Theoretical data set does not represent well in situ situations. Noise may not be optimum. More realistic conditions need to be included (e.g., comprehensive IOP data set being generated for PACE mission).

Figure 1-1: Estimated versus prescribed (black) and measured (red) APAR for selected models

APAR variability in the Northeast Asia Seas

-Multilinear R_w/R_{w0} APAR model was applied to SGLI imagery acquired over the Northeast Asia Seas (Bohai, Yellow, East China, Philippine Seas and Sea of Japan)

-Seasonal and interannual APAR variability was analyzed during the first 47 months of the GCOM-C mission (January 2018- November 2021).

-APAR seasonal, trend, and irregular components were described.

-Linear association between APAR and water variables (Chl-a, CDOM absorption coefficient,TSM, PAR) was examined.

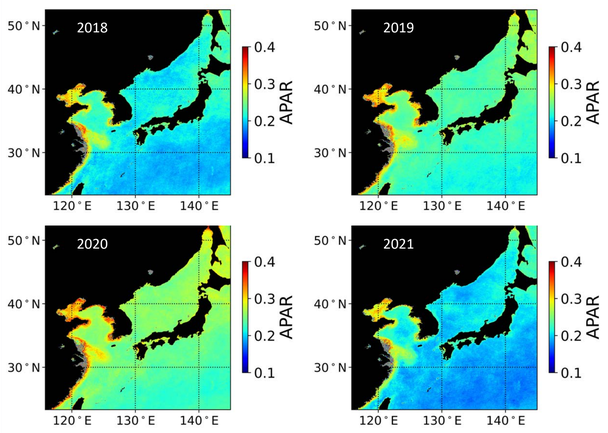

-At this annual scale, the APAR values range from 0.15 to 0.35, with the highest values obtained in the coastal regions of the Bohai, Yellow, and East China Seas.
-In the areas affected by the Yangtze and Yellow rivers, APAR is limited by the large amount of particulate inorganic material that reduce the probability of incident photons to be absorbed by chlorophyll.
-Along the coast of Japan, the offshore gradient of APAR is not as pronounced as expected in view of chlorophyll changes, because of compensation by absorption of CDOM and inorganic particles.
-Overall, APAR was higher in 2019 and especially 2020. It is not clear, however, how the changes in absorption by chlorophyll, CDOM, and inorganic particles combined to yield this tendency.

Figure 1-2: Annually averaged APAR for the Northeast Asia Seas in 2018, 2019, 2020, and 2021

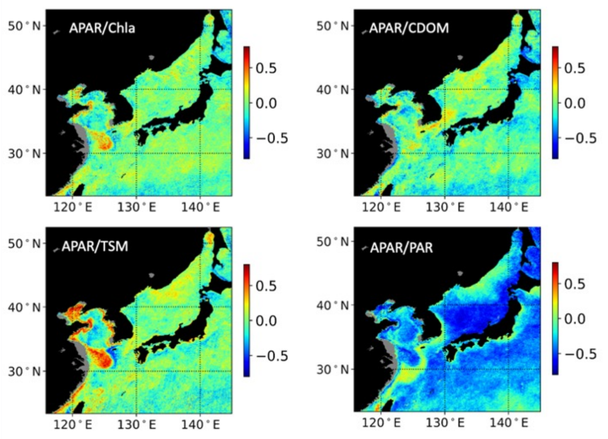

-Values are generally low (<0.2 in magnitude), especially for correlation between APAR and Chla and between APAR and a_{CDOM}, reflecting the fact that no single variable controls the APAR variability.

-In the Chinese coastal waters westward of the Kuroshio Branch Current west of Kyushu (KBCWK) and eastward of the Changjiang river diluted water, i.e., around 32°N and 125°E, the correlation is positive and relatively strong with Chla and TSM (probably dominated by organic particles), i.e., 0.4 and 0.6, respectively, suggesting that Chl controls APAR variability.

-The Pearson correlation between APAR and PAR is strong in some regions, for example strongly negative (about 0.5) in the lower part of the Sea of Japan (south of subpolar front and Tsushima Warm Current), suggesting that available light, by affecting water constituents and their IOPs, may contribute to APAR variability.

Figure 1-3: Pearson correlation coefficient for time series of APAR and Chla, a_{CDOM}, TSM, and PAR

APAR variability in the Northeast Asia Seas *(cont.)*

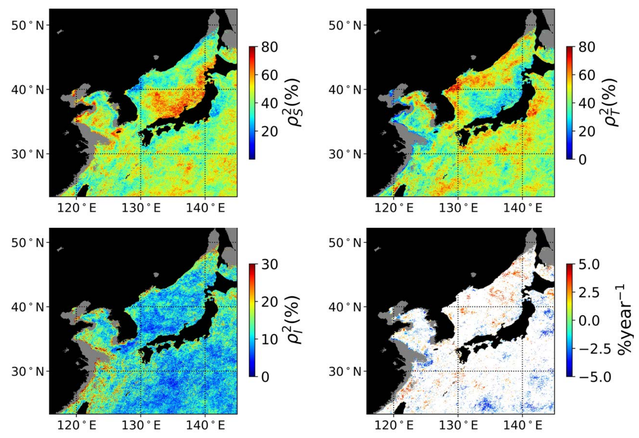

Figure 1-4: Relative contribution of trend, seasonal, and irregular component to total variance of 47-month APAR signal (%) and slope of the linear regression of the trend component (%/year)

-Seasonal component (50-60%) dominates in the southern part of the Sea of Japan (south of subpolar front), while the trend component (50-70%) controls variability along the coast of Russia (Liman and North Korean Cold Currents). At 40°N and 139°E, the trend represents 70% of the total variance and the seasonal component only 20%.

-In other regions, the seasonal and trend components contribute similarly to the total variance. The irregular component remains small everywhere, generally below 10%.

-The slope of a linear regression of the trend component over the 47-month time series is not significant in most of the study region, but there is a tendency for APAR to decrease by about 3% per year the Philippine Sea and the Northwest Pacific and to increase by 2 to 4% per year in the Sea of Japan.

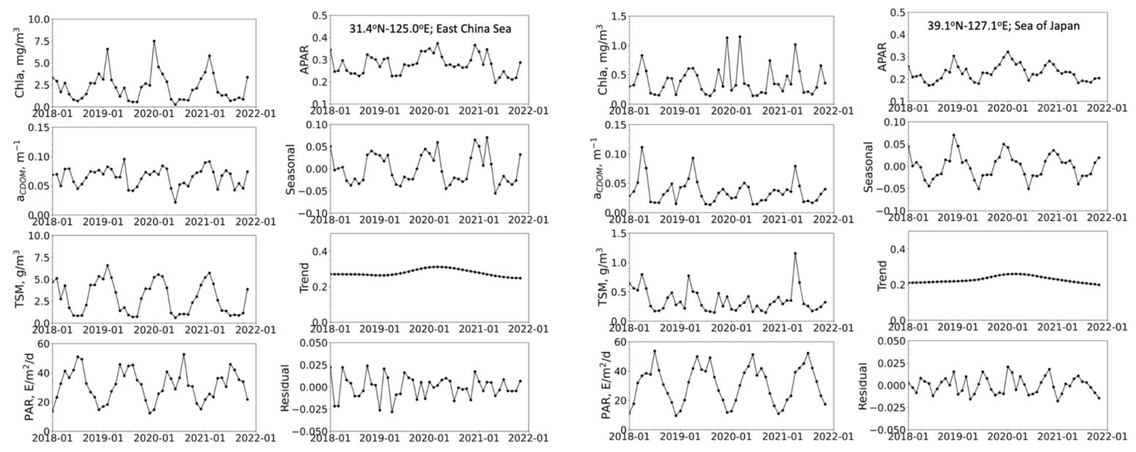

Figure 1-5: Time series of Chla, a_{CDOM}, TSM, PAR, and APAR and of components to the total APAR signal

-Seasonal cycle of Chla is large with values ranging from 0.1 to 8 mgm^{-3}. The seasonal cycle of CDOM absorption coefficient is less marked, but high values (i.e., > 0.07 m^{-1}) tend to occur when Chla is also high. The resulting picture is APAR exhibiting reduced seasonal variability, the trend component largely dominating, and the irregular component, moderately modulating seasonality of the total variance.

-Seasonal variability in characterized by peaks in spring and autumn, but the APAR time series, exhibits a single maximum during November-December. This is explained by the relatively high CDOM absorption coefficient during the spring blooms, which tends to reduce APAR during those blooms. The trend signal still dominates, but total signal has marked seasonal cycle.

2. Polarized water reflectance/particle assemblage

-Polarized water reflectance and degree of polarization DoP at 673 nm are sensitive to water composition and nature of phytoplankton assemblages.

-We derived DoP at 673 nm for SGLI imagery of 4 September 2020 over Northeast Asia Seas.

-SGLI polarized reflectance at 673 nm was corrected for Rayleigh scattering only. (A more accurate correction using SGLI-derived aerosol properties can be made.) DoP at 673 nm was related to TSM and Chla.

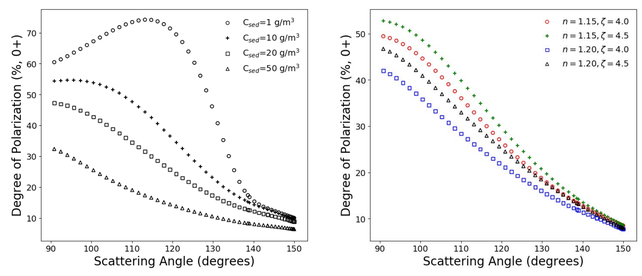

Figure 2-1: Left: Degree of polarization of the reflectance just above surface at 673 nm as a function of scattering angle for various sediment concentrations. Chlorophyll concentration is 0.1 mg/m3. Right: Degree of polarization of the reflectance just above surface for varied index of refraction and slope of the Junge distribution. Sediment concentration is 10 g/m³.

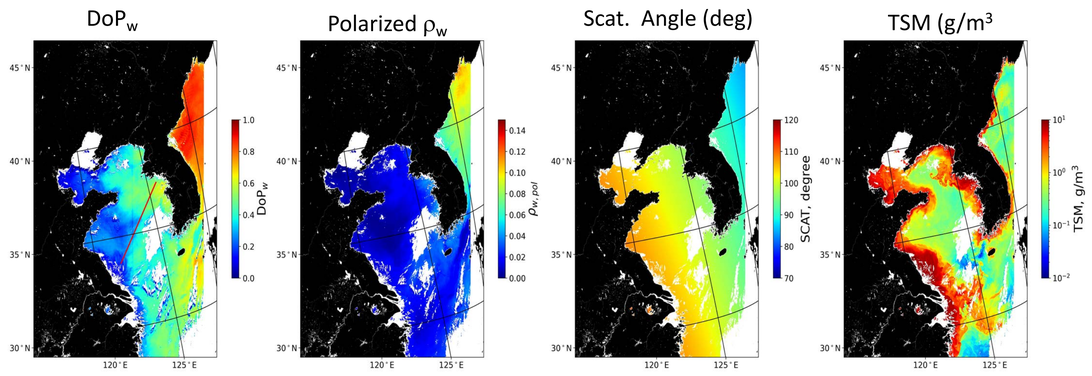

Figure 2-2: Retrieved DoP$_w$ and polarized ρ$_w$, SGLI 04 September 2022, Northeast Asia Seas

-DoP$_w$ is relatively large in Sea of Japan (relatively low Chla, small index of refraction, small particles, and scattering angle close to 90 deg).

-DoP$_w$ small along the coast of China where sediment concentration is large (relatively large index of refraction, large particles, and higher scattering angles).

-DoP$_w$ increases toward west coast of Korea, due to more organic particle assemblages (i.e., more phytoplankton) and increasing scattering angle.

-Polarized ρ$_w$ is small, with relatively small spatial contrast in entire Bohai and East China Seas, due to compensation between total ρ$_w$ and DoP$_w$ (e.g., high total ρ$_w$ by low DoP along the coast of China).

3. SOKOWASA bio-optical cruise

-Fiji, March 23 –April 3, 2022; R/V Alis; Chief Scientist: C. Dupouy (Co-I of SGLI investigation).

-20 stations with spectral UV-VIS $L_u(z)$, $E_d(z)$, R_{rs}, $b_{bp}(z)$ measurements, water sampling in euphotic zone for spectral a_p, a_{ph}, a_{CDOM}, CDOM fluorescence, HPLC pigments, PE, nutrients + glider for Chla fluorescence, turbidity, CDOM optical properties, temperature, salinity, currents.

-Objectives: Identification of phytoplankton enrichment sources in South Pacific; characterization of water optical properties.

-Cruise will provide data to develop APAR algorithm and evaluate ocean color products.

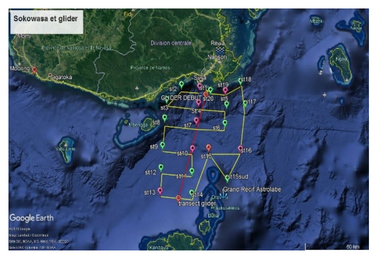

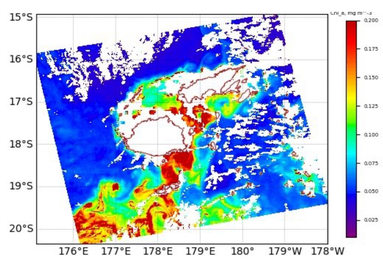

Acknowledgments. This work was supported by JAXA and NASA under various grants. We gratefully acknowledge all those involved in collecting, processing, and providing the in-situ datasets used in the study, in particular Prof. T. Hirawake and Dr. B. G. Mitchell. We also thank Dr. H. Murakami for helpful discussions and JAXA's EORC for generating and making available the SGLI ocean color products.